Recursive integral time extrapolation of elastic waves using low-rank symbol approximation[a]

[a]Published in Geophysical Journal International, 211, 1478-1493, (2017)

Junzhe Sun[*1], *Sergey Fomel*[1], *Yanadet Sripanich*[1] *and Paul Fowler*[2]

ABSTRACT

Conventional solutions of elastic wave equations rely on inaccurate finite-difference approximations of the time derivative, which result in strict dispersion and stability conditions and limitations. In this work, we derive a general solution to the elastic anisotropic wave equation, in the form of a Fourier Integral Operator (FIO). The proposed method is a generalization of the previously developed recursive integral time extrapolation operators from acoustic to elastic media, and can accurately propagate waves in time using the form of the analytical solution in homogeneous media. The formulation is closely connected to elastic wave mode decomposition, and can be applied to the most general anisotropic medium. The numerical calculation of the FIO makes use of a low-rank approximation to enable highly accurate and stable wave extrapolations. We present numerical examples including wave propagation in 3D heterogeneous orthorhombic and triclinic models.

INTRODUCTION

Elastic wave extrapolation honors elastic effects such as wave mode conversions, and provides reliable amplitude information which is crucial in seismic imaging of the subsurface. With advances of high-performance computing, seismic processing algorithms such as reverse-time migration (RTM) and full waveform inversion (FWI) based on elastic kernels are becoming more affordable (Lu et al., 2010; Vigh et al., 2014). The most widely used method to solve elastic wave equations involves finite-difference approximations of both spatial and temporal derivatives (Virieux, 1984, 1986; Etgen, 1987; Levander, 1988; Bernth and Chapman, 2010, 2011). The pseudospectral method (Kosloff et al., 1984; Reshef et al., 1988; Fornberg, 1996) provides accurate calculation of spatial derivatives, but still requires small time steps to avoid temporal dispersion. The numerical accuracy of temporal differentiation can be improved by employing higher-order Taylor expansions in the explicit case (Dablain, 1986; Crase, 1990) and Padé expansions in the implicit case (Chu, 2009; Liu and Sen, 2009). When implemented using coupled first-order particle velocity-stress systems, these methods usually require to use staggered grids to correctly center first-order differences of different model parameters (Özdenvar and McMechan, 1996; Corrêa et al., 2002; Bernth and Chapman, 2010). Recently, several methods have been introduced for stable and dispersion-free time extrapolation of scalar wavefields using the analytical solution of the acoustic wave equation in homogeneous media (Tal-Ezer, 1986; Tal-Ezer et al., 1987; Tabei et al., 2002; Etgen and Brandsberg-Dahl, 2009; Zhang and Zhang, 2009; Pestana and Stoffa, 2010; Chu and Stoffa, 2010; Fomel et al., 2013; Song et al., 2013; Fang et al., 2014;

Sun et al., 2016a). Du et al. (2014) provide a review of existing operators of such nature and refer to them as *recursive integral time extrapolation*. Chu and Stoffa (2011) and Firouzi et al. (2012) extend this approach to elastic wave extrapolation in isotropic media.

To mitigate cross-talk between P- and S-waves, it is often necessary to decouple different wave modes prior to imaging. In isotropic media, wave-mode separation can be achieved using the divergence and curl operators (Aki and Richards, 1980). Dellinger and Etgen (1990) implement wave-mode separation in anisotropic media by projecting the vector wavefield onto the polarization directions defined by the Christoffel equation. Yan and Sava (2009, 2012) implement wave-mode separation in vertical transversely isotropic (VTI) and tilted transverse isotropic (TTI) media by introducing space-domain non-stationary filters to handle spatial heterogeneity, and improve the efficiency using the idea of phase-shift plus interpolation (Yan and Sava, 2011). Zhang and McMechan (2010) further investigate wavefield vector decomposition method in the wavenumber domain and apply it to VTI media. Cheng and Fomel (2014) formulate the wave-mode separation and decomposition operators in heterogeneous media as Fourier Integral Operators (FIOs) and efficiently apply them using the low-rank approximation (Fomel et al., 2013). Sripanich et al. (2015) extend the low-rank decomposition operator to wave-mode decomposition in orthorhombic media.

Conventionally, wave-mode decomposition and wave extrapolation are considered as two separated steps. Hou et al. (2014) and Cheng et al. (2014, 2016) combine these two steps into a single FIO, which can be implemented by low-rank approximation. These methods are based on the assumption that the medium properties are sufficiently smooth so that their spatial derivatives can be neglected. However, the Earth model can be strongly heterogeneous and contain discontinuities, e.g., at salt/sediment boundaries. In such cases, the assumption about the smoothness of the Earth model is no longer valid and could lead to inaccurate calculation of polarization directions. More importantly, simultaneous wave extrapolation and wave-mode separation based on such an assumption may fail to provide reliable phase and amplitude information.

In this paper, we introduce a general framework for elastic wave extrapolation in strongly heterogeneous and anisotropic media without the assumption of the smoothness of the medium. The proposed method uses FIOs which allow accurate and stable wave extrapolation to be performed without explicit wave-mode separation. The proposed formulation reveals a simple connection between wave-mode decomposition and wave extrapolation through matrix exponentials. We also show that it is not necessary to explicitly decompose the wavefield into separate wave modes in order to apply recursive integral operators. We first derive one-step elastic wave extrapolation in homogeneous and smooth media motivated by one-step acoustic wave extrapolation (Zhang and Zhang, 2009; Sun et al., 2016a). In one-step extrapolation of elastic waves, only positive or negative frequency components are propagated, naturally providing the direction information that is useful for efficient wavefield up-down separation and angle gathers computation during imaging (Shen and Albertin, 2015; Hu et al., 2016; Sun et al., 2016a). We also construct the corresponding two-step scheme which uses only a real-valued vector wavefield. We draw connections of the proposed method to simultaneous propagation of decoupled elastic wave modes. Next, we show that to accurately model wave propagation in strongly heterogeneous media, spatial gradients of stiffnesses need to be included in the Christoffel matrix, leading to complex eigenvalues and polarization directions. Efficient calculation of the proposed FIOs in heterogeneous media is enabled by approximating the wave extrapolation matrix symbol with

a low-rank decomposition. Our numerical examples demonstrate that the proposed method is stable and free of dispersion artifacts and therefore is suitable for accurate elastic RTM and FWI in (strongly) heterogeneous anisotropic media.

THEORY

A Generic Wave Equation

Following the notation of Du et al. (2014), a generic linear second-order in time wave equation can be expressed in the following form

$$\left(\frac{\partial^2}{\partial t^2} + \mathbf{A}\right)\mathbf{u}(\mathbf{x},t) = 0\ , \tag{1}$$

where $\mathbf{u}$ is the wavefield, $\mathbf{x}$ is the spatial location, t is time, and $\mathbf{A}$ is the a matrix operator containing material parameters and spatial derivative operators. Equation 1 can also be expressed using the first-order system

$$\frac{\partial}{\partial t}\begin{bmatrix}\mathbf{u}\\ \mathbf{u}_t\end{bmatrix} = \begin{bmatrix}0 & \mathbf{I}\\ -\mathbf{A} & 0\end{bmatrix}\begin{bmatrix}\mathbf{u}\\ \mathbf{u}_t\end{bmatrix} \equiv \mathbf{B}\begin{bmatrix}\mathbf{u}\\ \mathbf{u}_t\end{bmatrix}\ , \tag{2}$$

where $\mathbf{u}_t \equiv \partial\mathbf{u}/\partial t$. The solution of equation 2 can be formulated using the definition of the matrix exponential:

$$\begin{bmatrix}\mathbf{u}(t)\\ \mathbf{u}_t(t)\end{bmatrix} = e^{\mathbf{B}t}\begin{bmatrix}\mathbf{u}(0)\\ \mathbf{u}_t(0)\end{bmatrix} \tag{3}$$

Defining $\Phi \equiv \sqrt{\mathbf{A}}$, the eigenvalue decomposition of $\mathbf{B}$ can be written as (Du et al., 2014)

$$\mathbf{B} = \S\Lambda\S^{-1}\ , \tag{4}$$

where

$$\begin{aligned}\S &= \tfrac{1}{\sqrt{2}}\begin{bmatrix}\mathbf{I} & \mathbf{I}\\ i\Phi & -i\Phi\end{bmatrix}\ ,\\ \S^{-1} &= \tfrac{1}{\sqrt{2}}\begin{bmatrix}\mathbf{I} & -i\Phi^{-1}\\ \mathbf{I} & i\Phi^{-1}\end{bmatrix}\ ,\\ \Lambda &= \begin{bmatrix}i\Phi & 0\\ 0 & -i\Phi\end{bmatrix}\ .\end{aligned} \tag{5}$$

The solution to the first-order system 3 can now be written as

$$\begin{bmatrix}\mathbf{u}(t)\\ \mathbf{u}_t(t)\end{bmatrix} = \S e^{\Lambda t}\S^{-1}\begin{bmatrix}\mathbf{u}(0)\\ \mathbf{u}_t(0)\end{bmatrix}\ . \tag{6}$$

To simplify the system, we can define the analytical wavefield

$$\begin{bmatrix}\hat{\mathbf{u}}_1(t)\\ \hat{\mathbf{u}}_2(t)\end{bmatrix} = \S^{-1}\begin{bmatrix}\mathbf{u}(t)\\ \mathbf{u}_t(t)\end{bmatrix} = \frac{1}{\sqrt{2}}\begin{bmatrix}\mathbf{u}(t) - i\Phi^{-1}\mathbf{u}_t(t)\\ \mathbf{u}(t) + i\Phi^{-1}\mathbf{u}_t(t)\end{bmatrix}\ . \tag{7}$$

The solution to equation 1 finally takes the form

$$\begin{bmatrix}\hat{\mathbf{u}}_1(t)\\ \hat{\mathbf{u}}_2(t)\end{bmatrix} = e^{\Lambda t}\begin{bmatrix}\hat{\mathbf{u}}_1(0)\\ \hat{\mathbf{u}}_2(0)\end{bmatrix} = \begin{bmatrix}e^{i\Phi t} & 0\\ 0 & e^{-i\Phi t}\end{bmatrix}\begin{bmatrix}\hat{\mathbf{u}}_1(0)\\ \hat{\mathbf{u}}_2(0)\end{bmatrix}\ . \tag{8}$$

Selecting the first of the two decoupled solutions of equation 8 leads to a time extrapolation operator

$$\hat{\mathbf{u}}(\mathbf{x}, t + \Delta t) = e^{i\Phi\Delta t}\hat{\mathbf{u}}(\mathbf{x}, t) \ , \tag{9}$$

where $\hat{\mathbf{u}} = (\mathbf{u} - i\Phi^{-1}\mathbf{u}_t)/\sqrt{2}$.

For acoustic isotropic constant-density wave equations for pressure waves, $\mathbf{A} = v^2|\mathbf{k}|^2$ where v is velocity and $|\mathbf{k}|^2$ is the Laplacian operator. This corresponds to the one-step extrapolation method proposed by (Zhang and Zhang, 2009).

The wavefield $\hat{\mathbf{u}}$ is an analytical signal, with its imaginary part being the Hilbert transform of its real part (Zhang and Zhang, 2009). To see this, we can perform Hilbert transform to the real-valued wavefield $\mathbf{u}$ in the frequency domain, and use the dispersion relation $\omega^2 = \Phi^2$ and derivative property of Fourier Transform

$$\mathbf{u}(t) \xrightarrow{\mathscr{F}} \mathbf{u}(\omega) \xrightarrow{\mathscr{H}} i\,\mathrm{sign}(\omega)\mathbf{u}(\omega) = \frac{i\,\omega}{|\omega|}\mathbf{u}(\omega) = \frac{i\,\omega}{\Phi}\mathbf{u}(\omega) \xrightarrow{\mathscr{F}^{-1}} = \Phi^{-1}\mathbf{u}_t(t) \ , \tag{10}$$

where $\mathscr{F}$ and $\mathscr{F}^{-1}$ denotes forward and inverse Fourier transform in time. The output corresponds to the imaginary part of analytical wavefield $\hat{\mathbf{u}}$.

Homogeneous Media

We first assume homogeneous model properties and investigate the form of time stepping solutions in general elastic media. For elastic anisotropic wave equations, the matrix operator $\mathbf{A}$ corresponds to the spatial Fourier transform of the matrix $-\Gamma/\rho = -\mathbf{DCD}^\intercal/\rho$, where Γ is the Christoffel matrix, ρ is density, $\mathbf{C}$ is the elastic stiffness tensor expressed in Voigt notation as a 6×6 matrix, and $\mathbf{D}$ is the derivative matrix operator give by

$$\mathbf{D} = \begin{bmatrix} \partial_x & 0 & 0 & 0 & \partial_z & \partial_y \\ 0 & \partial_y & 0 & \partial_z & 0 & \partial_x \\ 0 & 0 & \partial_z & \partial_y & \partial_x & 0 \end{bmatrix} \ . \tag{11}$$

In the Fourier (wavenumber) domain, the homogeneous $\mathbf{A}$ takes the form $\tilde{\Gamma}/\rho$ after i^2 cancels the negative sign, i.e., $-\Gamma \xrightarrow{\mathscr{F}} \tilde{\Gamma}$. For example, the Christoffel matrix $\tilde{\Gamma}$ in the case of orthorhombic anisotropy takes the form:

$$\tilde{\Gamma} = \begin{bmatrix} C_{11}k_x^2 + C_{66}k_y^2 + C_{55}k_z^2 & (C_{12} + C_{66})k_xk_y & (C_{13} + C_{55})k_xk_z \\ (C_{12} + C_{66})k_xk_y & C_{66}k_x^2 + C_{22}k_y^2 + C_{44}k_z^2 & (C_{23} + C_{44})k_yk_z \\ (C_{13} + C_{55})k_xk_z & (C_{23} + C_{44})k_yk_z & C_{55}k_x^2 + C_{44}k_y^2 + C_{33}k_z^2 \end{bmatrix} \ . \tag{12}$$

The square root matrix Φ is analogous to the phase function in the acoustic case, and corresponds to the angular frequency ω according to the dispersion relation. Since the matrix $\tilde{\Gamma}$ is symmetric positive definite (SPD), it can be diagonalized with its eigenvalues corresponding to the square of phase velocity of separate wave modes and its orthogonal eigenvectors corresponding to the polarization directions:

$$\begin{aligned} \mathbf{A} = \frac{\tilde{\Gamma}}{\rho} &= \mathbf{QVQ}^\intercal \\ &= \begin{bmatrix} \mathbf{a}_p & \mathbf{a}_{s1} & \mathbf{a}_{s2} \end{bmatrix} \begin{bmatrix} v_p^2k^2 & 0 & 0 \\ 0 & v_{s1}^2k^2 & 0 \\ 0 & 0 & v_{s2}^2k^2 \end{bmatrix} \begin{bmatrix} \mathbf{a}_p^\intercal \\ \mathbf{a}_{s1}^\intercal \\ \mathbf{a}_{s2}^\intercal \end{bmatrix} \ . \end{aligned} \tag{13}$$

Since $\mathbf{Q}$ is orthogonal, $\mathbf{Q}^\intercal$ projects the input vector to its column space. The square root of $\tilde{\Gamma}$ is found by taking the square root of the eigenvalues in the diagonal matrix. Analogously, the wave extrapolation operator, $e^{i\Phi\Delta t}$, can be computed as:

$$e^{i\Phi\Delta t} = \begin{bmatrix}\mathbf{a}_p & \mathbf{a}_{s1} & \mathbf{a}_{s2}\end{bmatrix} \begin{bmatrix} e^{iv_pk\Delta t} & 0 & 0 \\ 0 & e^{iv_{s1}k\Delta t} & 0 \\ 0 & 0 & e^{iv_{s2}k\Delta t} \end{bmatrix} \begin{bmatrix}\mathbf{a}_p^\intercal \\ \mathbf{a}_{s1}^\intercal \\ \mathbf{a}_{s2}^\intercal\end{bmatrix} . \tag{14}$$

An analogous idea of using matrix exponentials for wave propagation was studied previously by Kosloff and Kessler (1987) in application to the one-way wave equation. Physically, the operator in equation 14 first decomposes the input vector wavefield into three wave modes, phase shifts them using the corresponding phase velocities, and then aligns them in the polarization directions of the decomposed wave modes. The operator defined in equation 14 can be expressed as a summation of rank-one matrices

$$e^{i\Phi\Delta t} = \sum_{i=p,s1,s2} e^{iv_ik\Delta t}\mathbf{a}_i\mathbf{a}_i^\intercal . \tag{15}$$

Note that $\mathbf{a}_i\mathbf{a}_i^\intercal$ term in equation 15 is the wave mode decomposition operator (Dellinger, 1991; Zhang and McMechan, 2010).

In 3D, we can transform the input vector in the wavenumber domain $\hat{\mathbf{u}}(k) = \begin{bmatrix}\hat{u}_x(k) & \hat{u}_y(k) & \hat{u}_z(k)\end{bmatrix}^\intercal$. To apply the Fourier integral operator, we omit the pair of forward and backward Fourier transforms and formally write

$$\begin{aligned} e^{i\Phi\Delta t}\hat{\mathbf{u}}(k) &= \sum_{i=p,s1,s2} e^{iv_ik\Delta t}\mathbf{a}_i\mathbf{a}_i^\intercal\hat{\mathbf{u}} \\ &= \begin{bmatrix}\mathbf{a}_p & \mathbf{a}_{s1} & \mathbf{a}_{s2}\end{bmatrix} \begin{bmatrix} e^{iv_pk\Delta t} & 0 & 0 \\ 0 & e^{iv_{s1}k\Delta t} & 0 \\ 0 & 0 & e^{iv_{s2}k\Delta t} \end{bmatrix} \begin{bmatrix}\mathbf{a}_p^\intercal \\ \mathbf{a}_{s1}^\intercal \\ \mathbf{a}_{s2}^\intercal\end{bmatrix} \hat{\mathbf{u}} \\ &= \begin{bmatrix} s_{xx} & s_{xy} & s_{xz} \\ s_{yx} & s_{yy} & s_{yz} \\ s_{zx} & s_{zy} & s_{zz} \end{bmatrix} \hat{\mathbf{u}} , \end{aligned} \tag{16}$$

where

$$\begin{aligned} s_{xx} &= e^{iv_pk\Delta t}a_{p_x}a_{p_x} + e^{iv_{s1}k\Delta t}a_{s1_x}a_{s1_x} + e^{iv_{s2}k\Delta t}a_{s2_x}a_{s2_x} , \\ s_{xy} &= e^{iv_pk\Delta t}a_{p_x}a_{p_y} + e^{iv_{s1}k\Delta t}a_{s1_x}a_{s1_y} + e^{iv_{s2}k\Delta t}a_{s2_x}a_{s2_y} , \\ s_{xz} &= e^{iv_pk\Delta t}a_{p_x}a_{p_z} + e^{iv_{s1}k\Delta t}a_{s1_x}a_{s1_z} + e^{iv_{s2}k\Delta t}a_{s2_x}a_{s2_z} , \\ s_{yy} &= e^{iv_pk\Delta t}a_{p_y}a_{p_y} + e^{iv_{s1}k\Delta t}a_{s1_y}a_{s1_y} + e^{iv_{s2}k\Delta t}a_{s2_y}a_{s2_y} , \\ s_{yz} &= e^{iv_pk\Delta t}a_{p_y}a_{p_z} + e^{iv_{s1}k\Delta t}a_{s1_y}a_{s1_z} + e^{iv_{s2}k\Delta t}a_{s2_y}a_{s2_z} , \\ s_{zz} &= e^{iv_pk\Delta t}a_{p_z}a_{p_z} + e^{iv_{s1}k\Delta t}a_{s1_z}a_{s1_z} + e^{iv_{s2}k\Delta t}a_{s2_z}a_{s2_z} , \\ s_{yx} &= s_{xy} , \; s_{zx} = s_{xz} , \; s_{zy} = s_{yz} . \end{aligned} \tag{17}$$

Using the form of equation 9, we can also define the backward time extrapolator

$$\hat{\mathbf{u}}(\mathbf{x}, t - \Delta t) = e^{-i\Phi\Delta t}\hat{\mathbf{u}}(\mathbf{x}, t) . \tag{18}$$

If we require the data to be real-valued at every time step, and sum the forward and backward extrapolators, we arrive at the two-step formulation:

$$\hat{\mathbf{u}}(\mathbf{x}, t+\Delta t) = 2\,\cos(\Phi\Delta t)\hat{\mathbf{u}}(\mathbf{x}, t) - \hat{\mathbf{u}}(\mathbf{x}, t-\Delta t)\ . \tag{19}$$

According to equation 15, the cosine term has the following interpretation:

$$\begin{aligned} \cos(\Phi\Delta t) = & \quad e^{i\Phi\Delta t} + e^{-i\Phi\Delta t} \\ = & \sum_{i=p,s1,s2} (e^{iv_i k\Delta t} + e^{-iv_i k\Delta t})\mathbf{a}_i\mathbf{a}_i^{\mathsf{T}} \\ = & \sum_{i=p,s1,s2} 2\,\cos(v_i k\Delta t)\mathbf{a}_i\mathbf{a}_i^{\mathsf{T}}\ , \end{aligned} \tag{20}$$

and can be calculated as

$$\cos(\Phi\Delta t)\hat{\mathbf{u}}(k) = \begin{bmatrix} c_{xx} & c_{xy} & c_{xz} \\ c_{yx} & c_{yy} & c_{yz} \\ c_{zx} & c_{zy} & c_{zz} \end{bmatrix} \hat{\mathbf{u}}\ . \tag{21}$$

where

$$\begin{aligned} c_{xx} = & \cos(v_p k\Delta t)a_{p_x}a_{p_x} + \cos(v_{s1}k\Delta t)a_{s1_x}a_{s1_x} + \cos(v_{s2}k\Delta t)a_{s2_x}a_{s2_x}\ , \\ c_{xy} = & \cos(v_p k\Delta t)a_{p_x}a_{p_y} + \cos(v_{s1}k\Delta t)a_{s1_x}a_{s1_y} + \cos(v_{s2}k\Delta t)a_{s2_x}a_{s2_y}\ , \\ c_{xz} = & \cos(v_p k\Delta t)a_{p_x}a_{p_z} + \cos(v_{s1}k\Delta t)a_{s1_x}a_{s1_z} + \cos(v_{s2}k\Delta t)a_{s2_x}a_{s2_z}\ , \\ c_{yy} = & \cos(v_p k\Delta t)a_{p_y}a_{p_y} + \cos(v_{s1}k\Delta t)a_{s1_y}a_{s1_y} + \cos(v_{s2}k\Delta t)a_{s2_y}a_{s2_y}\ , \\ c_{yz} = & \cos(v_p k\Delta t)a_{p_y}a_{p_z} + \cos(v_{s1}k\Delta t)a_{s1_y}a_{s1_z} + \cos(v_{s2}k\Delta t)a_{s2_y}a_{s2_z}\ , \\ c_{zz} = & \cos(v_p k\Delta t)a_{p_z}a_{p_z} + \cos(v_{s1}k\Delta t)a_{s1_z}a_{s1_z} + \cos(v_{s2}k\Delta t)a_{s2_z}a_{s2_z}\ , \\ c_{yx} = & \quad c_{xy}\ ,\ c_{zx} = c_{xz}\ ,\ c_{zy} = c_{yz}\ . \end{aligned} \tag{22}$$

Note that, because the elements of the 3×3 matrix $\cos(\Phi\Delta t)$ in equation 21 are real-valued, the wavefield can stay real-valued as well. The matrix $\cos(\Phi\Delta t)$ is also closely connected with the k-space adjustment of the Christoffel matrix (Liu, 1995; Firouzi et al., 2012; Cheng et al., 2016).

Expanding the wave extrapolation operator in the form of equations 17 and 22 reveals a simple relationship between wave propagation and wave mode decomposition. In the one-step formulation, each individual term contained in each element of $e^{i\Phi\Delta t}$ is essentially a sequence of wave-mode decomposition, phase shift and recomposition. For example, the action of the first term in s_{xx}, $e^{iv_p k\Delta t}a_{p_x}a_{p_x}$, can be interpreted as projecting the x-component of a vector elastic wavefield onto the P-wave mode, phase shifting it using the P-wave phase velocity and then aligning it with the x-component of the P-wave polarization direction. If individual wave modes are needed to perform imaging, the decoupled operators can be separately applied. The operators concerning a specific wave mode are indicated by the corresponding phase velocity. The first columns in equations 17 and 22 are P-wave propagators, while the second and third columns are $S1$ and $S2$ wave propagators, respectively. In general anisotropic media beyond tilted transverse isotropic (TTI) symmetry, the two S-wave modes do not decouple easily. Therefore, in order to avoid S-wave singularities in wave propagation, the two coupled S-waves should be computed together (Sun et al., 2016a; Cheng et al., 2016).

The proposed framework, however, does not require explicit wave mode decomposition for wave extrapolation. Therefore, it can significantly reduce the computational cost of wave extrapolation, yet still obtain waves free of instability and dispersion artifacts. We also emphasize that the proposed method is capable of handling general anisotropic media, including the case of triclinic anisotropy.

Heterogeneous media

In heterogeneous media, the elastic wave equation can be expressed using the Einstein notation:

$$\rho \ddot{u}_i = (c_{ijkl} u_{k,l})_{,j} = c_{ijkl} u_{k,lj} + c_{ijkl,j} u_{k,l} \ , \tag{23}$$

where dot on top denotes time derivative, comma in subscript denotes spatial derivative and repeated indices imply summation. Analogously, the Christoffel matrix Γ in the case of orthorhombic symmetry can be expanded using the chain rule

$$\begin{aligned}
\Gamma &= \mathbf{D}\mathbf{C}(\mathbf{x})\mathbf{D}^{\mathsf{T}} \qquad (24)\\
&= \begin{bmatrix} \partial_x & 0 & 0 & 0 & \partial_z & \partial_y \\ 0 & \partial_y & 0 & \partial_z & 0 & \partial_x \\ 0 & 0 & \partial_z & \partial_y & \partial_x & 0 \end{bmatrix} \begin{bmatrix} C_{11} & C_{12} & C_{13} & 0 & 0 & 0 \\ C_{12} & C_{22} & C_{23} & 0 & 0 & 0 \\ C_{13} & C_{23} & C_{33} & 0 & 0 & 0 \\ 0 & 0 & 0 & C_{44} & 0 & 0 \\ 0 & 0 & 0 & 0 & C_{55} & 0 \\ 0 & 0 & 0 & 0 & 0 & C_{66} \end{bmatrix} \begin{bmatrix} \partial_x & 0 & 0 \\ 0 & \partial_y & 0 \\ 0 & 0 & \partial_z \\ 0 & \partial_z & \partial_y \\ \partial_z & 0 & \partial_x \\ \partial_y & \partial_x & 0 \end{bmatrix} \\
&= \begin{bmatrix} \partial_x & 0 & 0 & 0 & \partial_z & \partial_y \\ 0 & \partial_y & 0 & \partial_z & 0 & \partial_x \\ 0 & 0 & \partial_z & \partial_y & \partial_x & 0 \end{bmatrix} \begin{bmatrix} C_{11}\partial_x & C_{12}\partial_y & C_{13}\partial_z \\ C_{12}\partial_x & C_{22}\partial_y & C_{23}\partial_z \\ C_{13}\partial_x & C_{23}\partial_y & C_{33}\partial_z \\ 0 & C_{44}\partial_z & C_{44}\partial_y \\ C_{55}\partial_z & 0 & C_{55}\partial_x \\ C_{66}\partial_y & C_{66}\partial_x & 0 \end{bmatrix} \\
&= \begin{bmatrix} C_{11}\partial_x^2 + C_{66}\partial_y^2 + C_{55}\partial_z^2 & (C_{12}+C_{66})\partial_x\partial_y & (C_{13}+C_{55})\partial_x\partial_z \\ (C_{12}+C_{66})\partial_x\partial_y & C_{66}\partial_x^2 + C_{22}\partial_y^2 + C_{44}\partial_z^2 & (C_{23}+C_{44})\partial_y\partial_z \\ (C_{13}+C_{55})\partial_x\partial_z & (C_{23}+C_{44})\partial_y\partial_z & C_{55}\partial_x^2 + C_{44}\partial_y^2 + C_{33}\partial_z^2 \end{bmatrix} + \\
&\begin{bmatrix} \partial_x C_{11}\partial_x + \partial_y C_{66}\partial_y + \partial_z C_{55}\partial_z & \partial_x C_{12}\partial_y + \partial_y C_{66}\partial_x & \partial_x C_{13}\partial_z + \partial_z C_{55}\partial_x \\ \partial_y C_{12}\partial_x + \partial_x C_{66}\partial_y & \partial_x C_{66}\partial_x + \partial_y C_{22}\partial_y + \partial_z C_{44}\partial_z & \partial_y C_{23}\partial_z + \partial_z C_{44}\partial_y \\ \partial_z C_{13}\partial_x + \partial_x C_{55}\partial_z & \partial_z C_{23}\partial_y + \partial_y C_{44}\partial_z & \partial_x C_{55}\partial_x + \partial_y C_{44}\partial_y + \partial_z C_{33}\partial_z \end{bmatrix} .
\end{aligned}$$

After spatial Fourier transform, $-\Gamma \xrightarrow{\mathscr{F}} \tilde{\Gamma}$. The Christoffel matrix $\tilde{\Gamma}$ in the case of orthorhombic anisotropy takes the form:

$$\begin{aligned}
\tilde{\Gamma} &= \begin{bmatrix} C_{11}k_x^2 + C_{66}k_y^2 + C_{55}k_z^2 & (C_{12}+C_{66})k_x k_y & (C_{13}+C_{55})k_x k_z \\ (C_{12}+C_{66})k_x k_y & C_{66}k_x^2 + C_{22}k_y^2 + C_{44}k_z^2 & (C_{23}+C_{44})k_y k_z \\ (C_{13}+C_{55})k_x k_z & (C_{23}+C_{44})k_y k_z & C_{55}k_x^2 + C_{44}k_y^2 + C_{33}k_z^2 \end{bmatrix} - \qquad (25)\\
&i \begin{bmatrix} \partial_x C_{11}k_x + \partial_y C_{66}k_y + \partial_z C_{55}k_z & \partial_x C_{12}k_y + \partial_y C_{66}k_x & \partial_x C_{13}k_z + \partial_z C_{55}k_x \\ \partial_y C_{12}k_x + \partial_x C_{66}k_y & \partial_x C_{66}k_x + \partial_y C_{22}k_y + \partial_z C_{44}k_z & \partial_y C_{23}k_z + \partial_z C_{44}k_y \\ \partial_z C_{13}k_x + \partial_x C_{55}k_z & \partial_z C_{23}k_y + \partial_y C_{44}k_z & \partial_x C_{55}k_x + \partial_y C_{44}k_y + \partial_z C_{33}k_z \end{bmatrix} .
\end{aligned}$$

When the model is smoothly varying, which is the underlying assumption of wave mode separation (Cheng et al., 2014), the gradients of stiffnesses are insignificant. In such cases, the imaginary matrix can be dropped, which leads to the conventional real-valued Christoffel matrix in Equation 12. However, in the case of strong heterogeneity, such as at medium interfaces, the gradients of stiffnesses become significant and the imaginary part needs to be taken into account. Because $\tilde{\Gamma}$ becomes complex and non-Hermitian, the eigendecomposition of the generic matrix $\mathbf{A}$ is expressed as

$$\begin{aligned} \mathbf{A} = \frac{\tilde{\Gamma}}{\rho} = & \qquad \mathbf{Q}\mathbf{V}\mathbf{Q}^{-1} \\ = & \begin{bmatrix} \mathbf{a}_1 & \mathbf{a}_2 & \mathbf{a}_3 \end{bmatrix} \begin{bmatrix} \nu_1^2 & 0 & 0 \\ 0 & \nu_2^2 & 0 \\ 0 & 0 & \nu_3^2 \end{bmatrix} \begin{bmatrix} \hat{\mathbf{a}}_1^* \\ \hat{\mathbf{a}}_2^* \\ \hat{\mathbf{a}}_3^* \end{bmatrix} , \end{aligned} \tag{26}$$

where the superscript $*$ denotes conjugate transpose. Note that the eigenvalues ν_1^2 , ν_2^2 and ν_3^2, as well as their corresponding eigenvectors, are complex-valued. Since $\mathbf{Q}$ is square and $\mathbf{Q}^{-1}\mathbf{Q} = \mathbf{I}$:

$$\begin{cases} \hat{\mathbf{a}_i}^* \mathbf{a}_j = 1 \, , i = j \, ; \\ \hat{\mathbf{a}_i}^* \mathbf{a}_j = 0 \, , i \neq j \, . \end{cases}$$

Physically, this means in strongly heterogeneous media, wave mode separation cannot be clearly defined due to wave mode conversion, which is expressed as the imaginary part of eigenvalues. The polarization directions are no longer orthogonal in the real sense – they become orthogonal complex vectors.

The situation stated above does not prevent our framework from performing the correct wavefield extrapolation. The wave extrapolation operator then becomes

$$\begin{aligned} e^{i\Phi\Delta t}\hat{\mathbf{u}}(k) = & \sum_{i=1,2,3} e^{i\nu_i\Delta t}\mathbf{a}_i\hat{\mathbf{a}}_i^*\hat{\mathbf{u}} \\ = & \begin{bmatrix} \mathbf{a}_1 & \mathbf{a}_2 & \mathbf{a}_3 \end{bmatrix} \begin{bmatrix} e^{i\nu_1\Delta t} & 0 & 0 \\ 0 & e^{i\nu_2\Delta t} & 0 \\ 0 & 0 & e^{i\nu_3\Delta t} \end{bmatrix} \begin{bmatrix} \hat{\mathbf{a}}_1^* \\ \hat{\mathbf{a}}_2^* \\ \hat{\mathbf{a}}_3^* \end{bmatrix} \hat{\mathbf{u}} \\ = & \begin{bmatrix} \hat{s}_{xx} & \hat{s}_{xy} & \hat{s}_{xz} \\ \hat{s}_{yx} & \hat{s}_{yy} & \hat{s}_{yz} \\ \hat{s}_{zx} & \hat{s}_{zy} & \hat{s}_{zz} \end{bmatrix} \hat{\mathbf{u}} \, , \end{aligned} \tag{27}$$

where

$$\begin{aligned} \hat{s}_{xx} = & \; e^{i\nu_1\Delta t}a_{1_x}\hat{a}_{1_x} + e^{i\nu_2\Delta t}a_{2_x}\hat{a}_{2_x} + e^{i\nu_3\Delta t}a_{3_x}\hat{a}_{3_x} \, , \\ \hat{s}_{xy} = & \; e^{i\nu_1\Delta t}a_{1_x}\hat{a}_{1_y} + e^{i\nu_2\Delta t}a_{2_x}\hat{a}_{2_y} + e^{i\nu_3\Delta t}a_{3_x}\hat{a}_{3_y} \, , \\ \hat{s}_{xz} = & \; e^{i\nu_1\Delta t}a_{1_x}\hat{a}_{1_z} + e^{i\nu_2\Delta t}a_{2_x}\hat{a}_{2_z} + e^{i\nu_3\Delta t}a_{3_x}\hat{a}_{3_z} \, , \\ \hat{s}_{yx} = & \; e^{i\nu_1\Delta t}a_{1_y}\hat{a}_{1_x} + e^{i\nu_2\Delta t}a_{2_y}\hat{a}_{2_x} + e^{i\nu_3\Delta t}a_{3_y}\hat{a}_{3_x} \, , \\ \hat{s}_{yy} = & \; e^{i\nu_1\Delta t}a_{1_y}\hat{a}_{1_y} + e^{i\nu_2\Delta t}a_{2_y}\hat{a}_{2_y} + e^{i\nu_3\Delta t}a_{3_y}\hat{a}_{3_y} \, , \\ \hat{s}_{yz} = & \; e^{i\nu_1\Delta t}a_{1_y}\hat{a}_{1_z} + e^{i\nu_2\Delta t}a_{2_y}\hat{a}_{2_z} + e^{i\nu_3\Delta t}a_{3_y}\hat{a}_{3_z} \, , \\ \hat{s}_{zx} = & \; e^{i\nu_1\Delta t}a_{1_z}\hat{a}_{1_x} + e^{i\nu_2\Delta t}a_{2_z}\hat{a}_{2_x} + e^{i\nu_3\Delta t}a_{3_z}\hat{a}_{3_x} \, , \\ \hat{s}_{zy} = & \; e^{i\nu_1\Delta t}a_{1_z}\hat{a}_{1_y} + e^{i\nu_2\Delta t}a_{2_z}\hat{a}_{2_y} + e^{i\nu_3\Delta t}a_{3_z}\hat{a}_{3_y} \, , \\ \hat{s}_{zz} = & \; e^{i\nu_1\Delta t}a_{1_z}\hat{a}_{1_z} + e^{i\nu_2\Delta t}a_{2_z}\hat{a}_{2_z} + e^{i\nu_3\Delta t}a_{3_z}\hat{a}_{3_z} \, . \end{aligned} \tag{28}$$

Comparing equation 27 with equation 16, we can see that because the eigenvalues that appear in the exponent in equation 27 are no longer real-valued, the corresponding two-step operators to that in equation 20 cannot be constructed using Euler's formula.

Low-rank approximation

So far, we have laid out our basic theory of recursive integral time extrapolation of elastic waves. In mildly heterogeneous media, the Christoffel matrix is SPD. In strongly heterogeneous media, the Christoffel matrix becomes complex-valued and non-Hermitian. However, in both cases, the eigenvalues and eigenvectors of the Christoffel matrix become dependent on both spatial location and propagation direction, in other words, they are functions of both space $\mathbf{x}$ and wavenumber $\mathbf{k}$. If these operators are implemented straightforwardly, one is faced with the daunting task of computing and storing the complete eigenvalue decomposition of the Christoffel matrix using all the combinations of $\mathbf{x}$ and $\mathbf{k}$, leading to $\mathcal{O}(N_x^2)$ computational and memory complexity, where N_x refers to the total number of mesh points in 3D. To perform wave extrapolation in the form of integral operators, one would have to multiply matrices with vectors in dimension of N_x, leading to a computational complexity of $\mathcal{O}(N_x^2)$. This is simply infeasible for practical applications.

In this work, to efficiently apply the derived Fourier Integral Operators (FIOs), we proposed to apply the low-rank decomposition (Fomel et al., 2013) on the mixed-domain wave extrapolation matrices. Take the wave extrapolation operator in equation 27, $e^{i\Phi\Delta t}$, as an example. We propose to apply low-rank approximation on each individual element of its expansion. For instance, the $\hat{s}_{xx}$ element, which operates on the x-component of the input vector wavefield and outputs to the x-component of the output vector wavefield, can be approximated as (Fomel et al., 2013):

$$\hat{s}_{xx}(\mathbf{x},\mathbf{k}) \approx \sum_{m=1}^{M}\sum_{n=1}^{N} \hat{s}_{xx}(\mathbf{x},\mathbf{k}_m) a_{mn} \hat{s}_{xx}(\mathbf{x}_n,\mathbf{k}) \;, \tag{29}$$

where $\hat{s}_{xx}(\mathbf{x},\mathbf{k}_m) = \mathbf{U}$ and $\hat{s}_{xx}(\mathbf{x}_n,\mathbf{k}) = \mathbf{V}^*$ are sampled representative columns and rows from the original matrix $\hat{s}_{xx}(\mathbf{x},\mathbf{k}) = \mathbf{W}$, M and N are the numerical ranks of matrix $\mathbf{W}$, and the matrix $a_{mn} = \mathbf{A}$ is obtained from minimizing

$$\min_{\mathbf{A}} \|\mathbf{W} - \mathbf{U}\mathbf{A}\mathbf{V}^*\|_F \;. \tag{30}$$

Similarly, $\hat{s}_{xy}$ and $\hat{s}_{xz}$ can be approximated as:

$$\hat{s}_{xy}(\mathbf{x},\mathbf{k}) \approx \sum_{m=1}^{M}\sum_{n=1}^{N} \hat{s}_{xy}(\mathbf{x},\mathbf{k}_m) b_{mn} \hat{s}_{xy}(\mathbf{x}_n,\mathbf{k}) \;, \tag{31}$$

$$\hat{s}_{xz}(\mathbf{x},\mathbf{k}) \approx \sum_{m=1}^{M}\sum_{n=1}^{N} \hat{s}_{xz}(\mathbf{x},\mathbf{k}_m) c_{mn} \hat{s}_{xz}(\mathbf{x}_n,\mathbf{k}) \;. \tag{32}$$

The computation of $\hat{u}_x(\mathbf{x}, t+\Delta t)$ then becomes:

$$\begin{aligned}\hat{u}_x(\mathbf{x}, t+\Delta t) \approx & \sum_{m=1}^{M} \hat{s}_{xx}(\mathbf{x}, \mathbf{k}_m) \left(\sum_{n=1}^{N} a_{mn} \left(\int e^{i\mathbf{x}\mathbf{k}} \hat{s}_{xx}(\mathbf{x}_n, \mathbf{k}) \hat{u}_x(\mathbf{k}, t) d\mathbf{k} \right) \right) \\ + & \sum_{m=1}^{M} \hat{s}_{xy}(\mathbf{x}, \mathbf{k}_m) \left(\sum_{n=1}^{N} b_{mn} \left(\int e^{i\mathbf{x}\mathbf{k}} \hat{s}_{xy}(\mathbf{x}_n, \mathbf{k}) \hat{u}_y(\mathbf{k}, t) d\mathbf{k} \right) \right) \\ + & \sum_{m=1}^{M} \hat{s}_{xz}(\mathbf{x}, \mathbf{k}_m) \left(\sum_{n=1}^{N} c_{mn} \left(\int e^{i\mathbf{x}\mathbf{k}} \hat{s}_{xz}(\mathbf{x}_n, \mathbf{k}) \hat{u}_z(\mathbf{k}, t) d\mathbf{k} \right) \right) . \end{aligned} \tag{33}$$

The computation of y and z components can be carried out in a similar fashion. The computational cost of applying each FIO reduces to a complexity of $\mathcal{O}(NN_x \log N_x)$, where $\mathcal{O}(N_x \log N_x)$ is the complexity of one forward or inverse Fast Fourier Transform (FFT), and N is the numerical rank of the low-rank approximation, which is 1 for homogeneous media and $\mathcal{O}(1)$ for heterogeneous media.

Energy-norm imaging condition

The proposed method is well-suited for applications to elastic imaging and inversion using multi-component seismic data. In this section, we derive the energy-norm imaging condition using analytical wavefield, and show its connection to wave-mode decomposition.

The energy norm with respect to a SPD matrix $\mathbf{M}$ can be defined as:

$$e^2(\mathbf{u}) = ||\mathbf{u}||_{\mathbf{M}} = \mathbf{u}^\intercal \mathbf{M} \mathbf{u} . \tag{34}$$

In the acoustic case, the imaging condition based on the energy-norm is also referred to as the impedance sensitivity kernal (Zhu et al., 2009) or the inverse scattering imaging condition (Whitmore and Crawley, 2012):

$$I_a = \rho \mathbf{u}_t^\intercal \mathbf{w}_t + (v \nabla \mathbf{u})^\intercal (v \nabla \mathbf{w}) . \tag{35}$$

For general elastic media, the energy norm imaging condition can be expressed as (Kiyashchenko et al., 2007; Rocha et al., 2016)

$$I_e = \rho \mathbf{u}_t^\intercal \mathbf{w}_t + \mathbf{u}^\intercal \mathbf{D} \mathbf{C} \mathbf{D}^\intercal \mathbf{w} . \tag{36}$$

Using the analytic wavefield, equation 36 becomes

$$I_e = \rho(\mathbf{u}_t^\intercal \mathbf{w}_t + \mathbf{u}^\intercal \mathbf{A} \mathbf{w}) = \rho(\mathbf{u}_t^\intercal \mathbf{w}_t + \mathbf{u}^\intercal \Phi^\intercal \Phi \mathbf{w}) = \mathscr{R}\left[\rho (\Phi \hat{\mathbf{u}})^* (\Phi \hat{\mathbf{w}})\right] , \tag{37}$$

where $\mathscr{R}$ represents the operator of taking the real part. In a locally homogeneous medium, equation 37 can be expressed as

$$I_e = \mathscr{R}\left[\mathscr{F}^{-1}\left[\rho \hat{\mathbf{u}}^* \mathbf{A} \hat{\mathbf{w}}\right]\right] , \tag{38}$$

where $\mathscr{F}^{-1}$ represents inverse spatial Fourier transform. $\mathbf{A}$ is SPD and has the eigenvalue decomposition as equation 13, and the part in the wavenumber domain of equation 38 can be further expanded as

$$\begin{aligned}\rho \hat{\mathbf{u}}^* \mathbf{A} \hat{\mathbf{w}} = & \quad \rho \left(\mathbf{Q}^\intercal \hat{\mathbf{u}}\right)^* \mathbf{V} \mathbf{Q}^\intercal \hat{\mathbf{w}} \\ = & \begin{bmatrix} \hat{\mathbf{u}}_p^* & \hat{\mathbf{u}}_{s1}^* & \hat{\mathbf{u}}_{s2}^* \end{bmatrix} \begin{bmatrix} v_p^2 k^2 & 0 & 0 \\ 0 & v_{s1}^2 k^2 & 0 \\ 0 & 0 & v_{s2}^2 k^2 \end{bmatrix} \begin{bmatrix} \hat{\mathbf{w}}_p \\ \hat{\mathbf{w}}_{s1} \\ \hat{\mathbf{w}}_{s2} \end{bmatrix} \\ = & \sum_{i=p,s1,s2} v_i^2 k^2 \hat{\mathbf{u}}_i^* \hat{\mathbf{w}}_i . \end{aligned} \tag{39}$$

Equation 39 corresponds to the summation of the image produced by three pure wave-mode reflections (P-P, S1-S1 and S2-S2 images) using the formula prescribed in equations 35. Therefore, the proposed framework provides the possibility of individually accessing the contribution of each wave-mode in the elastic energy-norm imaging condition, in addition to outputing their summation.

The imaging condition prescribed in equation 38 is the cross-correlation of two positive-frequency analytical wavefields. This corresponds to the back-scattering part of the wavefield. If one instead performs cross-correlation between two wavefield with opposite signs of frequency, e.g. $\mathbf{u}^*$ only contains negative frequency and $\mathbf{w}$ only contains positive frequency, it will lead to a different forward-scattering imaging condition

$$I_t = \mathscr{R}\left[\mathscr{F}^{-1}\left[\rho\hat{\mathbf{u}}\mathbf{A}\hat{\mathbf{w}}\right]\right] = \rho(-\mathbf{u}_t^\intercal\mathbf{w}_t + \mathbf{u}^\intercal\mathbf{A}\mathbf{w}) \ . \tag{40}$$

The forward-scattering imaging condition corresponds to the tomographic correlation between two wavefields. It is conventionally treated as low-frequency noise in RTM, but is what FWI needs for performing low-frequency updates in the velocity gradient Díaz and Sava (2012, 2013); Ramos-Martinez et al. (2016). Equation 40 can also be expanded in a similar fashion as equation 39 to access individual contributions from each wave mode.

It is important to note that the inverse- and forward-scattering imaging conditions using scalar and vector analytical wavefields discussed in this section are not restricted to one-step wave extrapolation. There are different ways of obtaining an analytical wavefield using conventional finite-different or pseudo-spectral wave extrapolation, for example, by separately propagating a wavefield using a Hilbert-transformed source wavelet (Shen and Albertin, 2015; Hu et al., 2016) and use it as the imaginary part of the analytical wavefield.

NUMERICAL EXAMPLES

In this section, we use various synthetic models to test the one-step version of the proposed low-rank RITE method.

We first test the accuracy and stability of the proposed method in a two-layer orthorhombic model, and compare it with the conventional finite-difference and pseudospectral methods. We construct a two-layer orthorhombic model on a $100 \times 100 \times 100$ grid with the density-normalized stiffness tensor (in km^2/s^2) of the first layer given in equation 41 (Schoenberg and Helbig, 1997), and the second layer being a scaled version of the first layer by a factor of 1.8. We apply triangle smoothing in the vertical direction with a radius of 4. The spatial sampling rate in all directions of the grid is 10 m. A displacement source is oriented at 45° tilt and 45° azimuth and injected at $x = 0.5\ km,\ y = 0.5\ km\ , z = 0.4\ km$. The source wavelet has a peak frequency of 35 Hz. A wavefield snapshot shown in Figure 3 was taken at 0.18 s. The wavefield that was modeled by eighth-order finite-difference in space and second-order finite-difference in time using a time-step size of 1 ms suffers from strong dispersion artifacts (Figure 1a), while the wavefield modeled by pseudospectral method in space and second-order finite-difference in time is free of spatial dispersions. However, increasing the time step size to 2 ms leads to numerical instability of both methods, and thus the results are not shown. In comparison, the proposed low-rank RITE method shows an accurate result free from dispersion and instability using increasing time step sizes of 1 ms,

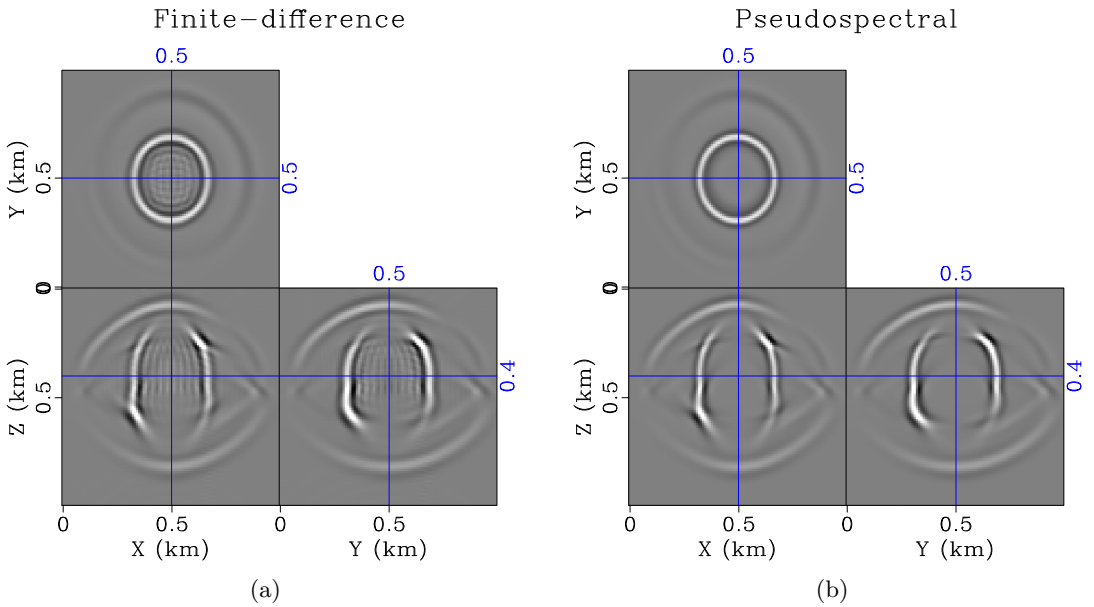

Figure 1: Wavefield snapshot of wavefield propagation in a two-layer orthorhombic model using the finite-difference method (a) and the pseudospectral method (b) with a step size of 1 ms. twolayer3d/ ORTw-fd-1,ORTw-ps-1

2 ms, 4 ms and 8 ms (Figure 3).

$$\begin{bmatrix} 9 & 3.6 & 2.25 & 0 & 0 & 0 \\ 3.6 & 9.84 & 2.4 & 0 & 0 & 0 \\ 2.25 & 2.4 & 5.9375 & 0 & 0 & 0 \\ 0 & 0 & 0 & 2 & 0 & 0 \\ 0 & 0 & 0 & 0 & 1.6 & 0 \\ 0 & 0 & 0 & 0 & 0 & 2.182 \end{bmatrix} \tag{41}$$

Next, to test wave extrapolation accuracy at a medium interface, where strong heterogeneity occurs, we use the same two-layer orthorhombic model without smoothing in the vertical direction. Figure 3 shows wavefield snapshots taken at $t = 0.18$ s. Because of the strong contrast at the medium interface, the transmitted and reflected waves calculated by the proposed method including the stiffness gradient terms demonstrates noticeable amplitude and phase differences compared with the waves calculated by ignoring the gradient terms. Figure 4a shows interleaved shot gathers extracted at $Z = 100$ m, which compares the modeled data by the low-rank method and the pseudo-spectral method, both with and without accounting for the stiffness gradient terms. We can observe that for either the low-rank or the pseudo-spectral methods, modeled direct P- and S-arrivals are identical while reflected P- and S-arrivals show obvious difference in both amplitude and phase due to the missing of stiffness gradient terms. To validate our observation, we also carry out wave extrapolation using the pseudo-spectral method by solving first- and second-order elastic wave equations. Their shot gather, shown in Figure 4b, demonstrates the same phenomena. Finally, in Figure 4c, we interleave the amplitude-normalized shot gathers from low-rank RITE solution including the stiffness gradients, togethr with a pseudo-spectral solution of

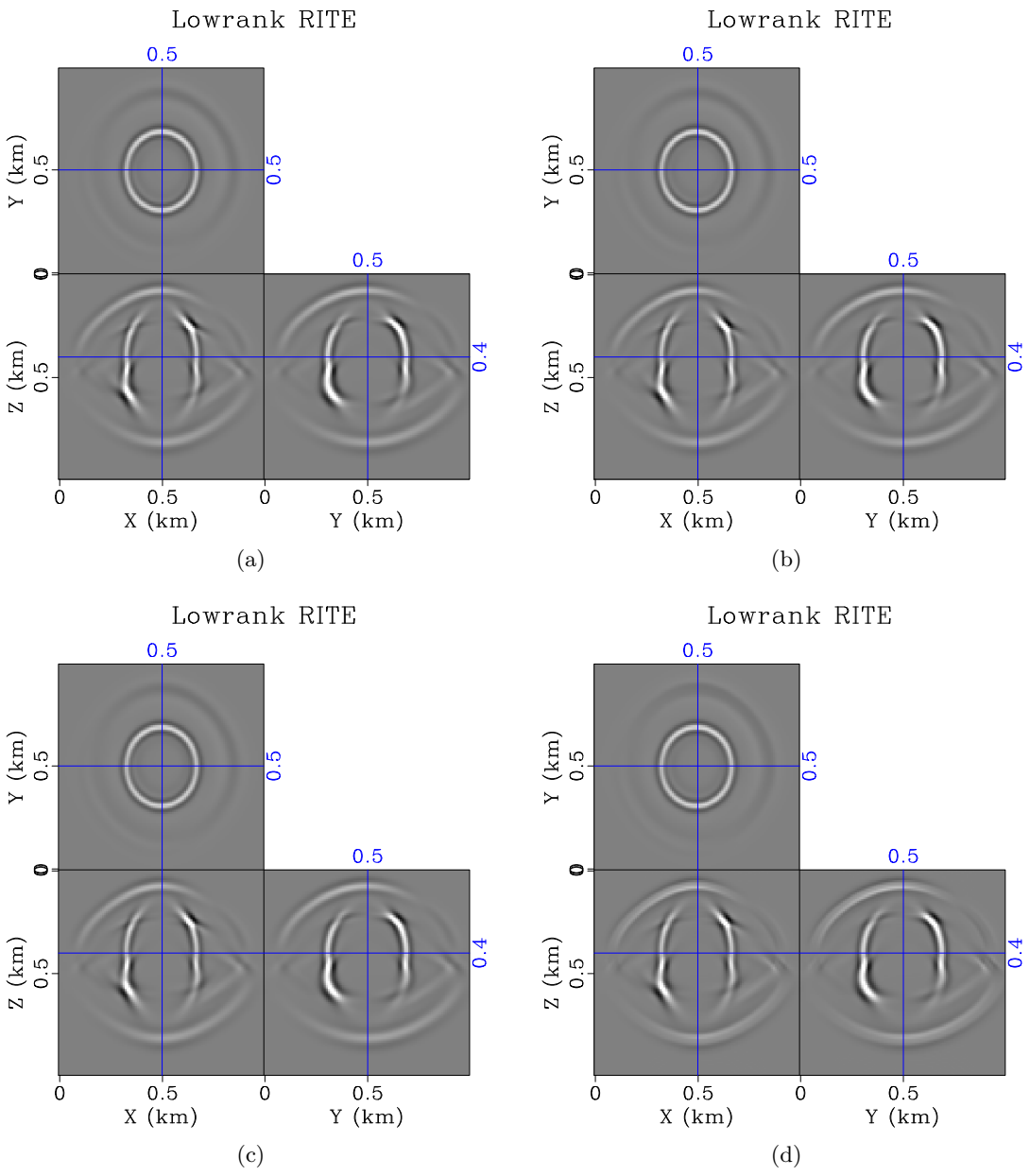

Figure 2: Wavefield snapshot of wavefield propagation in a two-layer orthorhombic model using the proposed low-rank RITE method with a step size of 1 ms (a), 2 ms (b), 4 ms (c) and 8 ms (d). twolayer3d/ ORTw-lr-1,ORTw-lr-2,ORTw-lr-4,ORTw-lr-8

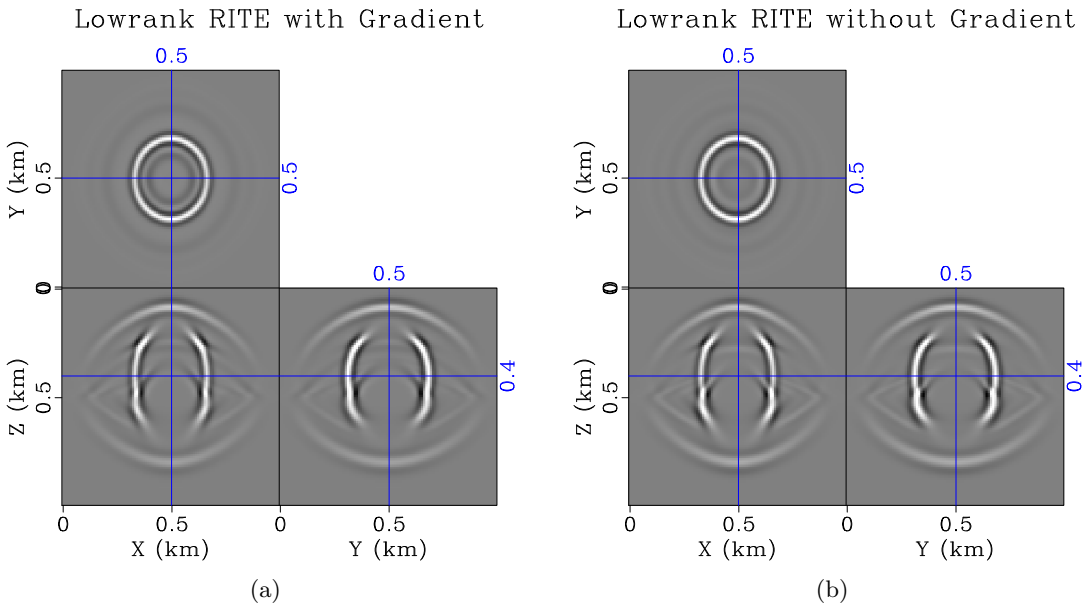

Figure 3: Wavefield snapshot of wavefield propagation in a two-layer orthorhombic model using the low-rank RITE method with (a) and without (b) accounting for the gradient of stiffnesses. gradient/ ORTw-lr-1,ORTw-lr0-1

the first-order equations. They demonstrate almost identical amplitude and phase behavior. In terms of computational cost, the numerical ranks of the wave extrapolation matrices are 2 when the stiffness gradient terms are not included, while the ranks increase to 5 when the gradient terms are included.

In the third example, we test the ability of the proposed method to model decomposed wave mode propagation in a more general anisotropic medium, a triclinic medium. We use the lab measurements from Mah and Schmitt (2003) as the background model, with the stiffness tensors (in GPa) of the triclinic model shown in equation 42, which is then normalized by a mass density of 1.395 kg/m^3. We then add spherical perturbations centered at $Z = 400\ m, X = 500\ m, Y = 500\ m$ to all the density normalized stiffness tensors to make the models mildly heterogeneous. Using the same mesh size as the previous example, and a time step size of 1 ms, the proposed method is capable of accurately and separately propagating P- and S-waves in the triclinic medium (Figure 5) using equation 16. The two S-wave modes are propagated together since they do not decouple easily. Both the P- and coupled S-waves are free of numerical dispersion and instablity. The numercial ranks of the wave extrapolation matrices for this test are 3.

$$\begin{bmatrix} 14.9 & 6.3 & 5.2 & 0.7 & 0.9 & -0.5 \\ 6.3 & 14.9 & 5.7 & 0.8 & 1.5 & -0.4 \\ 5.2 & 5.7 & 10.0 & 0.7 & 0.8 & 0.1 \\ 0.7 & 0.8 & 0.7 & 3.3 & -0.1 & 0.1 \\ 0.9 & 1.5 & 0.8 & -0.1 & 3.0 & 0.2 \\ -0.5 & -0.4 & 0.1 & 0.1 & 0.2 & 3.7 \end{bmatrix} \tag{42}$$

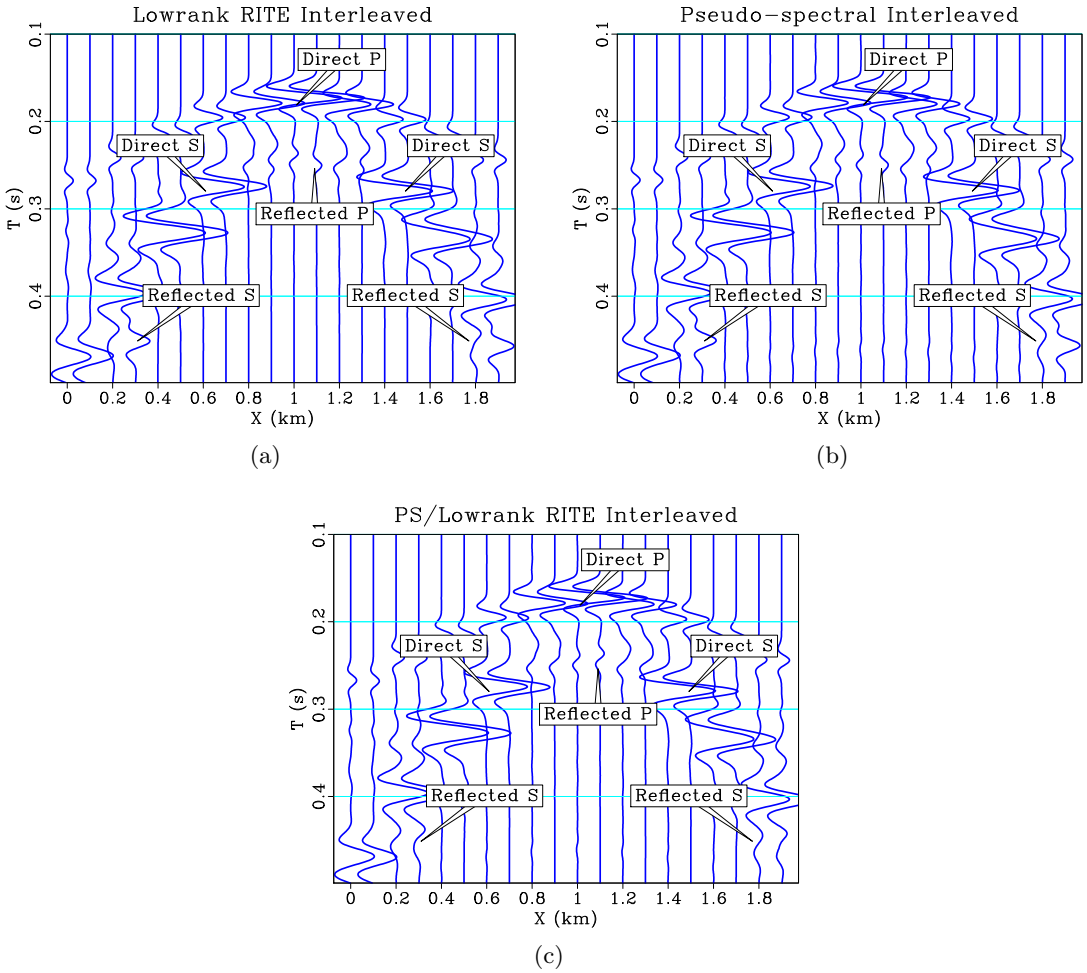

Figure 4: Interleaved shot gathers extracted at $Z = 100\ m$ between wavefield modeled by (a) the low-rank method with and without including the stiffness gradient terms; (b) the pseudo-spectral method with and without including the stiffness gradient terms; and (c) the pseudo-spectral method and the low-rank method, both including the stiffness gradient terms. The odd-numbered traces correspond to the methods mentioned first. gradient/ inter-lr,inter-ps,inter-pslr

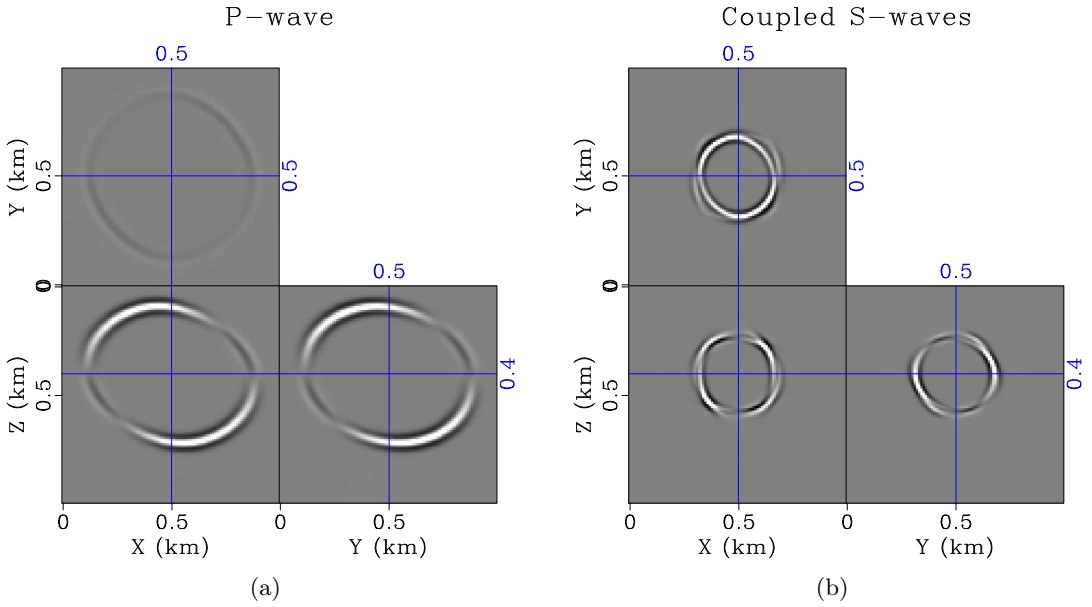

Figure 5: Wavefield snapshot of (a) P-wave and (b) coupled S-waves propagation in a perturbed triclinic model using the proposed low-rank RITE method with a step size of 1 ms. homotric3d-dc/ TRIw-lr-p,TRIw-lr-s

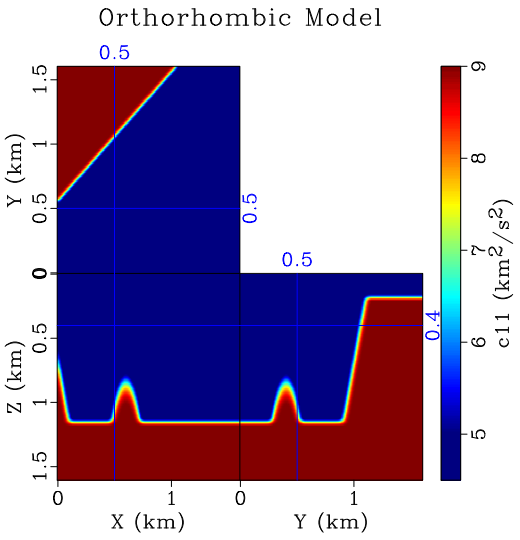

Figure 6: (a) $C11$ of an orthorhommic model based on the French model. french-dc/ ORTc-11-f

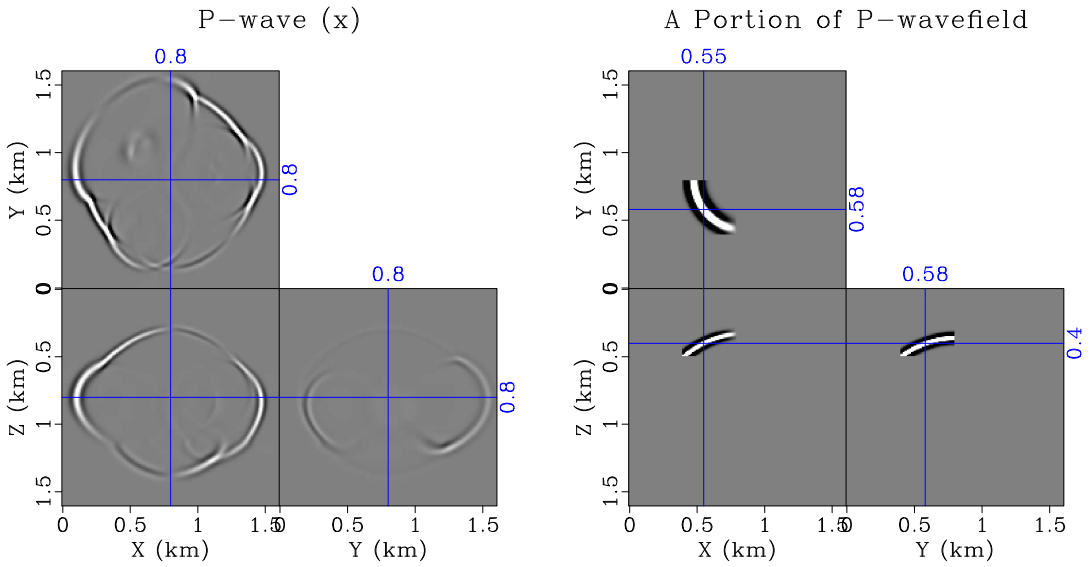

Figure 7: (a) The x-component of decoupled P-wavefield at $t = 0.39s$. (b) A portion of the wavefield centered at $Z = 0.64\ km, X = 0.89\ m, Y = 0.93\ m$. french-dc/ ORTw-lr-p-x,snap-p-x-cut

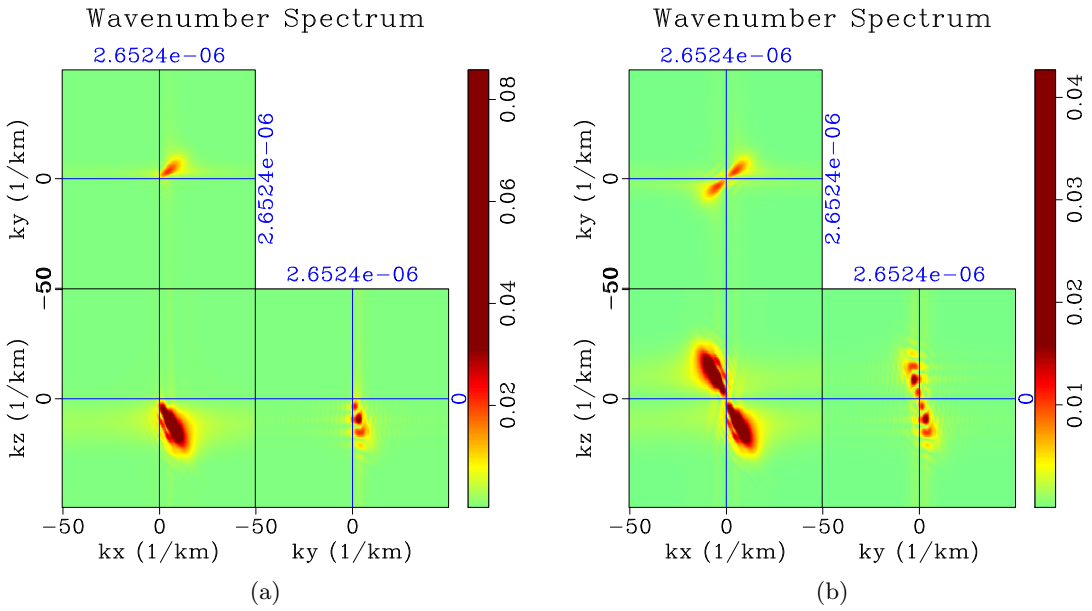

Figure 8: Wavenumber amplitude spectrum of (a) the analytical wavefield, and (b) its real part. french-dc/ freq-p-x,freq-p-x2

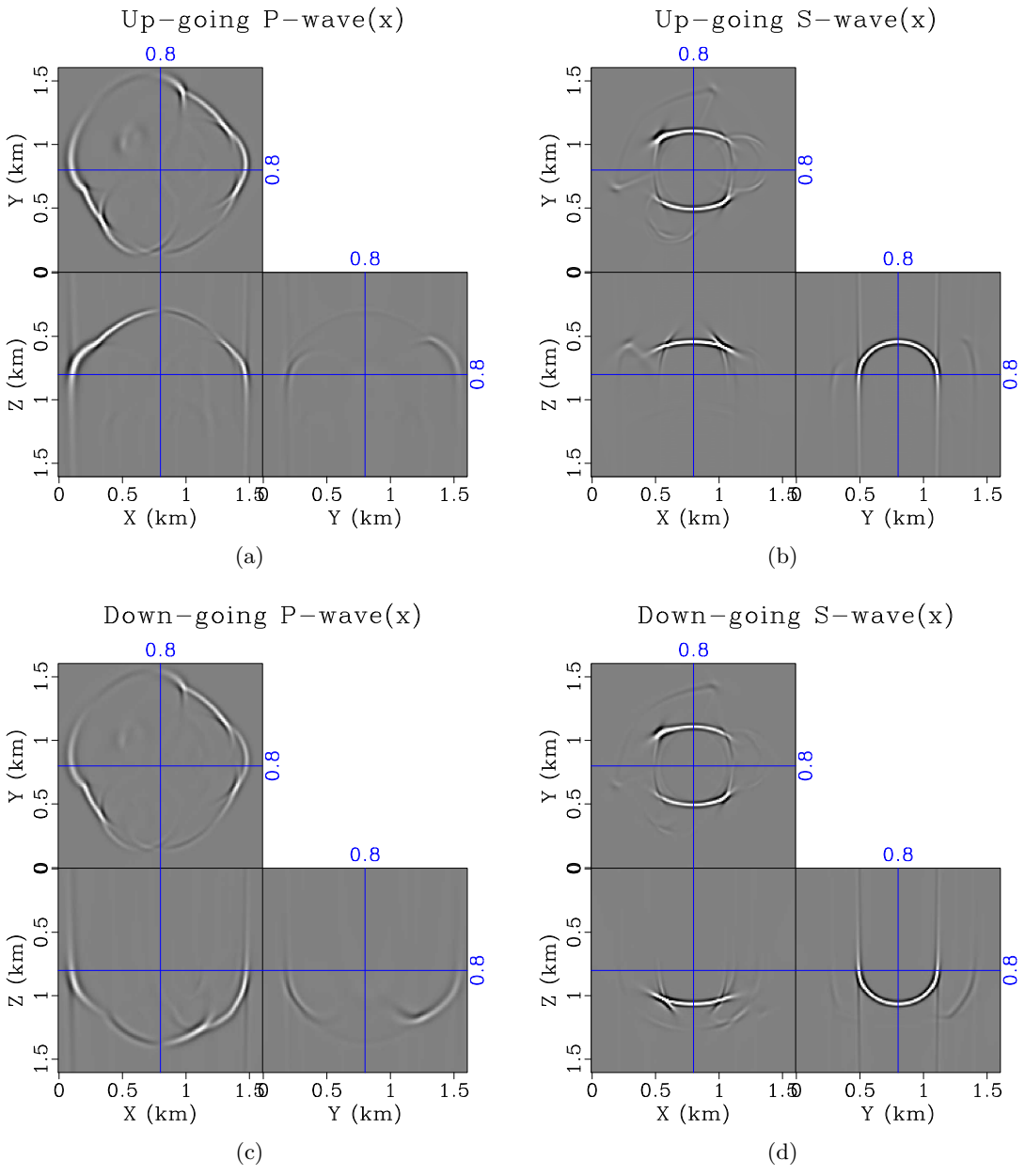

Figure 9: The decomposition of wavefield into up- and down-going directions. (a) The up-going P-wave, and (b) the up-going S-wave. (c) The down-going P-wave. (d) The down-going S-wave. french-dc/ snap-p-x-up,snap-s-x-up,snap-p-x-dn,snap-s-x-dn

In the last example, we demonstrate one advantage of the proposed method for seismic imaging applications, the accessibility of directional information of wavefield. For a real-valued wavefield, the propagation direction cannot be uniquely defined in the wavenumber domain because of its symmetric wavenumber spectrum about zero (Hu et al., 2016). This is due to the fact that the real-valued wavefield contains both positive and negative frequency components. The analytical wavefield, on the other hand, has decoupled positive and negative frequency components, so its wavenumber spectrum reveals the direction of wavefield propagation. To demonstrate this fact, we construct an orthorhombic model based on the French model (French, 1974), with its $C11$ component shown in Figure 6. We use equation 16 to calculate a decoupled P-wavefield, whose x-component at $t = 0.39\ s$ is shown in Figure 7a. We select a portion of the wavefield centered at $Z = 0.4\ km, X = 0.58\ m, Y = 0.58\ m$ propagating in the direction negative along all three axes, as shown in Figure 7b. Figure 8a shows the wavenumber amplitude spectrum of the wavefield, and its energy are all distributed in the positive octant. One the other hand, the wavenumber amplitude spectrum of the real part of the wavefield shows symmetric distribution of energy about the origin, as demonstrated by Figure 8b. Finally, we decouple the upward-traveling and downward-traveling wavefield based on the sign k_z, and the downward-traveling P- and S-waves are shown in Figure 9c and 9d.

DISCUSSION

In this paper, we have considered second-order displacement equations for elastic wave extrapolation. However, the framework presented here is not limited to such a formulation. For example, second-order stress equations can be used, which has the advantage of not calculating spatial derivative of stiffnesses. Other first-order formulations should also be investigated.

Our formulation can be viewed as an extension of the one-step extrapolation method by Zhang and Zhang (2009) to elastic anisotropic media. It has been shown by Bleistein et al. (2008) that the one-step solution is asymptotically true amplitude, i.e., it provides the same traveltime and leading order amplitude as conventional acoustic wave propagation. It is reasonable to expect that the new formulation for elastic waves has similar behavior. However, more rigorous theoretical proof is required to arrive at a definitive conclusion.

In the last numerical example, we have demonstrated that our method is advantageous in providing directional information about the wavefield. This allows for efficient computation of wavefield up-down separation, RTM angle gathers and absorbing boundary conditions (Shen and Albertin, 2015; Hu et al., 2016; Sun et al., 2016b) in the context of elastic imaging.

CONCLUSIONS

We have presented a recursive integral time extrapolation method for modeling elastic wave propagation in general heterogeneous anisotropic media. The one-step formulation involves analytical wavefields that contain either positive or negative frequencies, which provides crucial information about the direction of wave propagation. The two-step formulation, on the other hand, involves only real-valued wavefields. The proposed method employs a low-rank approximation to efficiently apply the Fourier integral operators defined by the

mixed-domain components of the modified Christoffel matrix. In practice, this reduces the computational cost to a small number of spatial fast Fourier transforms per time step. The low-rank decomposition only needs to be computed once prior to wave extrapolation. Numerical examples show that the proposed method has superior accuracy and stability compared with conventional finite-difference and pseudospectral methods.

ACKNOWLEDGEMENTS

We thank Jiubing Cheng for helpful discussions and thank the sponsors of the Texas Consortium for Computational Seismology for financial support. The first and third authors were additionally supported by the Statoil Fellows Program at the University of Texas at Austin. We thank the Texas Advanced Computing Center for providing computational resources used in this study.

REFERENCES

Aki, K., and P. G. Richards, 1980, Quantitative seismology: W.H. Freeman & Co.

Bernth, H., and C. Chapman, 2010, A comparison of finite-difference grids for anisotropic elastic modelling: 80th Annual International Meeting, SEG, Expanded Abstracts, 2916–2920.

———, 2011, A comparison of the dispersion relations for anisotropic elastodynamic finite-difference grids: Geophysics, **76**, no. 3, WA43–WA50.

Bleistein, N., Y. Zhang, and G. Zhang, 2008, Asymptotically true-amplitude one-way wave equations in t: modeling, migration and inversion: 78th Annual International Meeting, SEG, Expanded Abstracts, 2292–2296.

Cheng, J., T. Alkhalifah, Z. Wu, P. Zou, and C. Wang, 2016, Simulating propagation of decoupled elastic waves using low-rank approximate mixed-domain integral operators for anisotropic media: Geophysics, **81**, no. 2, T63–T77.

Cheng, J., and S. Fomel, 2014, Fast algorithms for elastic-wave-mode separation and vector decomposition using low-rank approximation for anisotropic media: Geophysics, **79**, no. 4, C97–C110.

Cheng, J., Z. Wu, and T. Alkhalifah, 2014, Simulating propagation of decomposed elastic waves using low-rank approximate mixed-domain integral operators for heterogeneous transversely isotropic media: 84th Annual International Meeting, SEG, Expanded Abstracts, 3393–3399.

Chu, C., 2009, Seismic modeling and imaging with the Fourier method: PhD thesis, The University of Texas at Austin.

Chu, C., and P. L. Stoffa, 2010, Acoustic anisotropic wave modeling using normalized pseudo-Laplacian: 80th Annual International Meeting, SEG, Expanded Abstracts, 2972–2976.

———, 2011, Application of normalized pseudo-Laplacian to elastic wave modeling on staggered grids: Geophysics, **76**, no. 5, T113–T121.

Corrêa, G. J. P., M. Spiegelman, S. Carbotte, and J. C. Mutter, 2002, Centered and staggered fourier derivatives and hilbert transforms: GEOPHYSICS, **67**, 1558–1563.

Crase, E., 1990, High-order (space and time) finite-difference modeling of the elastic wave equation: 60th Annual International Meeting, SEG, Expanded Abstracts, 987–991.

Dablain, M. A., 1986, The application of high-order differencing to the scalar wave equation: Geophysics, **51**, 54–66.

Dellinger, J., and J. Etgen, 1990, Wave-field separation in two-dimensional anisotropic media: Geophysics, **55**, no. 7, 914–919.

Dellinger, J. A., 1991, Anisotropic Seismic Wave Propagation: PhD thesis, Stanford University.

Díaz, E., and P. Sava, 2012, Understanding the reverse time migration backscattering: noise or signal?, *in* SEG Technical Program Expanded Abstracts 2012: SEG, 1–6.

———, 2013, Wavefield tomography using rtm backscattering, *in* SEG Technical Program Expanded Abstracts 2013: SEG, 4021–4026.

Du, X., P. J. Fowler, and R. P. Fletcher, 2014, Recursive integral time-extrapolation methods for waves: A comparative review: Geophysics, **79**, no. 1, T9–T26.

Etgen, J., and S. Brandsberg-Dahl, 2009, The pseudo-analytical method: application of pseudo-Laplacians to acoustic and acoustic anisotropic wave propagation: 79th Annual International Meeting, SEG, Expanded Abstracts, 2552–2556.

Etgen, J. T., 1987, Finite-difference elastic anisotropic wave propagation: Stanford Exploration Project Report, **56**, 23–58.

Fang, G., S. Fomel, Q. Du, and J. Hu, 2014, Lowrank seismic wave extrapolation on a staggered grid: Geophysics, **79**, no. 3, T157–T168.

Firouzi, K., B. T. Cox, B. E. Treeby, and N. Saffari, 2012, A first-order k-space model for elastic wave propagation in heterogeneous media: The Journal of the Acoustical Society of America, **132**, 1271–1283.

Fomel, S., L. Ying, and X. Song, 2013, Seismic wave extrapolation using lowrank symbol approximation: Geophysical Prospecting, **61**, no. 3, 526–536.

Fornberg, B., 1996, A practical guide to pseudospectral methods: Cambridge University Press. (Cambridge Books Online).

French, W. S., 1974, Two-dimensional and three-dimensional migration of model-experiment reflection profiles: Geophysics, **39**, no. 3, 265–277.

Hou, S., Q. Du, and G. Fang, 2014, Elastic wavefield extrapolation based on wavefield vector decomposition and lowrank decomposition: 84th Annual International Meeting, SEG, Expanded Abstracts, 3411–3416.

Hu, J., H. Wang, and X. Wang, 2016, Angle gathers from reverse time migration using analytic wavefield propagation and decomposition in the time domain: Geophysics, **81**, no. 1, S1–S9.

Kiyashchenko, D., R.-E. Plessix, B. Kashtan, and V. Troyan, 2007, A modified imaging principle for true-amplitude wave-equation migration: Geophysical Journal International, **168**, no. 3, 1093–1104.

Kosloff, D., and D. Kessler, 1987, Accurate depth migration by a generalized phase–shift method: Geophysics, **52**, no. 8, 1074–1084.

Kosloff, D., M. Reshef, and D. Loewenthal, 1984, Elastic wave calculations by the Fourier method: Bulletin of the Seismological Society of America, **74**, no. 3, 875–891.

Levander, A., 1988, Fourth–order finite–difference P-SV seismograms: Geophysics, **53**, no. 11, 1425–1436.

Liu, Q.-H., 1995, Generalization of the k-space formulation to elastodynamic scattering problems: The Journal of the Acoustical Society of America, **97**, no. 3, 1373–1379.

Liu, Y., and M. K. Sen, 2009, An implicit staggered-grid finite-difference method for seismic modelling: Geophysical Journal International, **179**, no. 1, 459–474.

Lu, R., J. Yan, P. Traynin, J. E. Anderson, and T. Dickens, 2010, Elastic RTM: anisotropic

wave-mode separation and converted-wave polarization correction: 80th Annual International Meeting, SEG, Expanded Abstracts, 3171–3175.

Mah, M., and D. R. Schmitt, 2003, Determination of the complete elastic stiffnesses from ultrasonic phase velocity measurements: Journal of Geophysical Research: Solid Earth, **108**, no. B1, ECV 6–1–ECV 6–11.

Özdenvar, T., and G. A. McMechan, 1996, Causes and reduction of numerical artefacts in pseudo-spectral wavefield extrapolation: Geophysical Journal International, **126**, 819–828.

Pestana, R. C., and P. L. Stoffa, 2010, Time evolution of the wave equation using rapid expansion method: Geophysics, **75**, no. 4, T121–T131.

Ramos-Martinez, J., N. Chemingui, S. Crawley, Z. Zou, A. Valenciano, and E. Klochikhina, 2016, A robust fwi gradient for high-resolution velocity model building: 86th Annual International Meeting, SEG, Expanded Abstracts, 1258–1262.

Reshef, M., D. Kosloff, M. Edwards, and C. Hsiung, 1988, Three-dimensional elastic modeling by the Fourier method: Geophysics, **53**, no. 9, 1184–1193.

Rocha, D., N. Tanushev, and P. Sava, 2016, Isotropic elastic wavefield imaging using the energy norm: Geophysics, **81**, no. 4, S207–S219.

Schoenberg, M., and K. Helbig, 1997, Orthorhombic media: Modeling elastic wave behavior in a vertically fractured earth: Geophysics, **62**, no. 6, 1954–1974.

Shen, P., and U. Albertin, 2015, Up-down separation using Hilbert transformed source for causal imaging condition: 85th Annual International Meeting, SEG, Expanded Abstracts, 4175–4179.

Song, X., S. Fomel, and L. Ying, 2013, Lowrank finite-differences and lowrank Fourier finite-differences for seismic wave extrapolation: Geophysical Journal International, **193**, no. 2, 960–969.

Sripanich, Y., S. Fomel, J. Sun, and J. Cheng, 2015, Elastic wave-vector decomposition in orthorhombic media: 85th Annual International Meeting, SEG, Expanded Abstracts, 498–503.

Sun, J., S. Fomel, and L. Ying, 2016a, Low-rank one-step wave extrapolation for reverse time migration: GEOPHYSICS, **81**, S39–S54.

———, 2016b, Lowrank one-step wave extrapolation for reverse-time migration: Geophysics, **81**, no. 1, S39–S54.

Tabei, M., T. D. Mast, and R. C. Waag, 2002, A k-space method for coupled first-order acoustic propagation equations: The Journal of the Acoustical Society of America, **111**, no. 1, 53–63.

Tal-Ezer, H., 1986, Spectral methods in time for hyperbolic equations: SIAM Journal on Numerical Analysis, **23**, no. 1, 11–26.

Tal-Ezer, H., D. Kosloff, and Z. Koren, 1987, An accurate scheme for seismic forward modelling: Geophysical Prospecting, **35**, no. 5, 479–490.

Vigh, D., K. Jiao, D. Watts, and D. Sun, 2014, Elastic full-waveform inversion application using multicomponent measurements of seismic data collection: Geophysics, **79**, no. 2, R63–R77.

Virieux, J., 1984, SH-wave propagation in heterogeneous media: Velocity-stress finite-difference method: Geophysics, **49**, no. 11, 1933–1942.

———, 1986, P-SV wave propagation in heterogeneous media: Velocity-stress finite-difference method: Geophysics, **51**, no. 4, 889–901.

Whitmore, N. D., and S. Crawley, 2012, Applications of rtm inverse scattering imaging conditions, *in* SEG Technical Program Expanded Abstracts 2012: SEG, 1–6.

Yan, J., and P. Sava, 2009, Elastic wave-mode separation for VTI media: Geophysics, **74**, no. 5, WB19–WB32.

———, 2011, Improving the efficiency of elastic wave-mode separation for heterogeneous tilted transverse isotropic media: Geophysics, **76**, no. 4, T65–T78.

———, 2012, Elastic wave mode separation for tilted transverse isotropic media: Geophysical Prospecting, **60**, 29–48.

Zhang, Q., and G. A. McMechan, 2010, 2D and 3D elastic wavefield vector decomposition in the wavenumber domain for VTI media: Geophysics, **75**, no. 3, D13–D26.

Zhang, Y., and G. Zhang, 2009, One-step extrapolation method for reverse time migration: Geophysics, **74**, no. 4, A29–A33.

Zhu, H., Y. Luo, T. Nissen-Meyer, C. Morency, and J. Tromp, 2009, Elastic imaging and time-lapse migration based on adjoint methods: Geophysics, **74**, no. 6, WCA167–WCA177.